EB1 and EB3 promote cilia biogenesis by several centrosome-related mechanisms

Jacob M. Schrøder[1], Jesper Larsen[1], Yulia Komarova[2], Anna Akhmanova[3,*], Rikke I. Thorsteinsson[1], Ilya Grigoriev[3], Robert Manguso[1], Søren T. Christensen[1], Stine F. Pedersen[1], Stefan Geimer[4,‡] and Lotte B. Pedersen[1,‡]

[1]Department of Biology, University of Copenhagen, Universitetsparken 13, DK-2100 Copenhagen, Denmark
[2]Department of Pharmacology, University of Illinois College of Medicine, 835 S. Wolcott Avenue, Chicago, IL 60612, USA
[3]Department of Cell Biology, Erasmus Medical Center, 3000 CA Rotterdam, The Netherlands
[4]Cell Biology/Electron Microscopy, University of Bayreuth, Universitätsstr. 30, 95440 Bayreuth, Germany
*Present address: Cell Biology, Faculty of Science, Utrecht University, Padualaan 8, 3584 CH, Utrecht, The Netherlands
‡Authors for correspondence (Stefan.Geimer@uni-bayreuth.de; LBPedersen@bio.ku.dk)

Accepted 4 April 2011
Journal of Cell Science 124, 2539-2551

doi:10.1242/jcs.085852

Summary

The microtubule (MT) plus-end-tracking protein EB1 is required for assembly of primary cilia in mouse fibroblasts, but the mechanisms involved and the roles of the related proteins EB2 and EB3 in ciliogenesis are unknown. Using protein depletion experiments and expression of dominant-negative constructs we show here that EB1 and EB3, but not EB2, are required for assembly of primary cilia in cultured cells. Electron microscopy and live imaging showed that cells lacking EB1 or EB3 are defective in MT minus-end anchoring at the centrosome and/or basal body, and possess abnormally short cilia stumps surrounded by vesicles. Further, GST pull-down assays, mass spectrometry and immunoprecipitation indicated that EB1 and EB3 interact with proteins implicated in MT minus-end anchoring or vesicular trafficking to the cilia base, suggesting that EB1 and EB3 promote ciliogenesis by facilitating such trafficking. In addition, we show that EB3 is localized to the tip of motile cilia in bronchial epithelial cells and affects the formation of centriole-associated rootlet filaments. Collectively, our findings indicate that EBs affect biogenesis of cilia by several centrosome-related mechanisms and support the idea that different EB1–EB3 dimer species have distinct functions within cells.

Key words: EB1, EB3, Cilia, Basal body, Microtubule, Centriole

Introduction

Primary cilia are sensory organelles that project from the surface of most growth-arrested mammalian cells, and are crucial for controlling multiple cellular and developmental processes, including cell growth, differentiation, tissue patterning and homeostasis (Berbari et al., 2009; Christensen et al., 2007). Mutations leading to dysfunctional cilia can lead to a variety of diseases and developmental disorders, referred to as ciliopathies (Fliegauf et al., 2007). Primary cilia consist of a microtubule (MT) axoneme that extends from a modified centriole, the basal body, and is surrounded by a bilayer lipid membrane enriched for specific membrane receptors and ion channels, such as platelet-derived growth factor receptor α and components of the Hedgehog and Wingless (Wnt) signaling pathways (Berbari et al., 2009; Christensen et al., 2007). Assembly of primary cilia is thought to involve trafficking of post-Golgi vesicles to the cilium base, where the vesicles are exocytosed and their ciliary cargo transported into the growing cilium by intraflagellar transport (Nachury et al., 2010; Pedersen and Rosenbaum, 2008). Central to the trafficking of vesicles to the cilium base are the intraflagellar transport protein 20 (IFT20) (Follit et al., 2006) and the small GTPase Rab11 (Knödler et al., 2010; Westlake et al., 2011). Rab11 associates with Rabin8, the GTP exchange factor for Rab8, and is required for targeting Rabin8 to the centrosome in a MT-dependent manner (Westlake et al., 2011). In turn, Rabin8 is associated with Rab8 and a complex of proteins called the BBSome – owing to its association with the cilium-related Bardet-Biedl Syndrome (BBS) (Nachury et al., 2007). BBS proteins localize to pericentriolar satellites and interact with pericentriolar matrix protein 1 (PCM1), and inactivation or depletion of BBS proteins, PCM1, Rab8 or Rab11 results in failure to assemble cilia and/or to target specific proteins to the cilium compartment (Berbari et al., 2008; Nachury et al., 2007). Depletion or inactivation of proteins involved in MT minus-end anchoring at the centrosome (e.g. ninein) or in the docking of vesicles to the distal end of the basal body (e.g. Cep164 and ODF2) results in similar ciliogenesis defects (Graser et al., 2007; Ishikawa et al., 2005). Despite these advances and the identification of several additional proteins involved in ciliogenesis (Pedersen et al., 2008), many questions remain unanswered. For example, although multiple centrosomal proteins with ciliogenic functions have been described (Pedersen et al., 2008), the specific mechanism by which many of these proteins promote ciliogenesis is unknown.

We have shown recently that the MT plus-end tracking protein (+TIP) EB1 is required for assembly of primary cilia in mouse fibroblasts (Schrøder et al., 2007), but the mechanism(s) involved and the roles of the related proteins EB2 and EB3 in ciliogenesis are unclear. EBs comprise a conserved family of MT +TIPs that have important roles in regulating MT dynamics (Akhmanova and Steinmetz, 2008; Schuyler and Pellman, 2001). Mammals contain three EBs, which are similar in structure (EB1, EB2, and EB3; 57–66% amino acid identity) and are encoded by separate genes (Juwana et al., 1999; Su and Qi, 2001). All three EBs exist as homodimers in vivo and in vitro, and EB1 and EB3 also form a heterodimeric complex that might be functionally distinct from the homodimers

(De Groot et al., 2010; Komarova et al., 2009). EBs contain an N-terminal MT-binding calponin homology (CH) domain, a flexible linker and a C-terminal coiled-coil domain region that mediates EB dimerization and partially overlaps with a unique EB homology domain (Akhmanova and Steinmetz, 2008; De Groot et al., 2010; Hayashi and Ikura, 2003; Honnappa et al., 2005; Komarova et al., 2009; Slep et al., 2005). The EB homology domain is followed by a tail of 20–30 amino acid residues that frequently ends with the sequence EEY/F (Honnappa et al., 2005; Slep et al., 2005). Both the EB homology domain and the EEY/F motif are important for association of EBs with their binding partners, such as dynactin subunit p150^{Glued}, cytoplasmic linker protein (CLIP) 170, adenomatous polyposis coli (APC) and mitotic centromere-associated kinesin (MCAK; also known as KIF2C) (Akhmanova and Steinmetz, 2008). Although many proteins bind to all three EBs, the affinity with which they bind to individual EBs can vary. For example, CLIP170, CLIP115 and MCAK bind directly to EB1 and EB3, but display very low affinity for EB2 (Komarova et al., 2005; Lee et al., 2008), whereas specific interactions with the F-actin binding protein drebin and the E3 ubiquitin ligase SIAH-1 were reported for EB3, but not for EB1 and EB2 (Ban et al., 2009; Geraldo et al., 2008). Functional analyses of mammalian EBs have mainly focused on EB1 and EB3, and have primarily been studied in the context of MT plus ends. These studies have shown that EB1 and EB3 exhibit a substantial degree of redundancy, although specific differences were also reported (Akhmanova and Steinmetz, 2008). For example, EB1 and EB3 both affect CLIP localization at the growing end of MTs and promote persistent MT growth by suppressing catastrophes (Komarova et al., 2005; Komarova et al., 2009). However, EB3 seems to have a unique role in neuritogenesis (Geraldo et al., 2008).

Here, we report that EB1 and EB3, but not EB2, are required for assembly of primary cilia in human foreskin fibroblasts (hFFs) and retinal pigment epithelial (RPE) cells. By using a variety of approaches, we provide evidence that EB1 and EB3 affect cilia formation through MT minus-end anchoring at the basal body, in turn facilitating vesicular trafficking to the cilium base. In addition, we provide evidence that EB3 has a role in the regulation of cilia length and the formation of centriole-associated rootlet filaments.

Results

Depletion of EB1 or EB3, but not EB2, inhibits cilia formation

To address the roles of EBs in ciliogenesis, we used small interfering RNAs (siRNAs) to deplete EB1, EB2 or EB3 from hFFs, and serum starved confluent cells to induce ciliogenesis. Western blot analysis by using rat monoclonal EB antibodies (Komarova et al., 2005) confirmed the efficiency of siRNA treatment (Fig. 1A), and immunofluorescence microscopy (IFM) revealed that EB1- or EB3-depleted cultures contained 50% fewer ciliated cells than mock-transfected or EB2-depleted cultures, as determined by staining with antibody against detyrosinated α-tubulin (Glu-tub) (Fig. 1B,C). Similar results were obtained in RPE cells (32% ciliated cells in EB1/EB3-depleted cultures compared to 66% ciliated cells in cultures treated with mock or

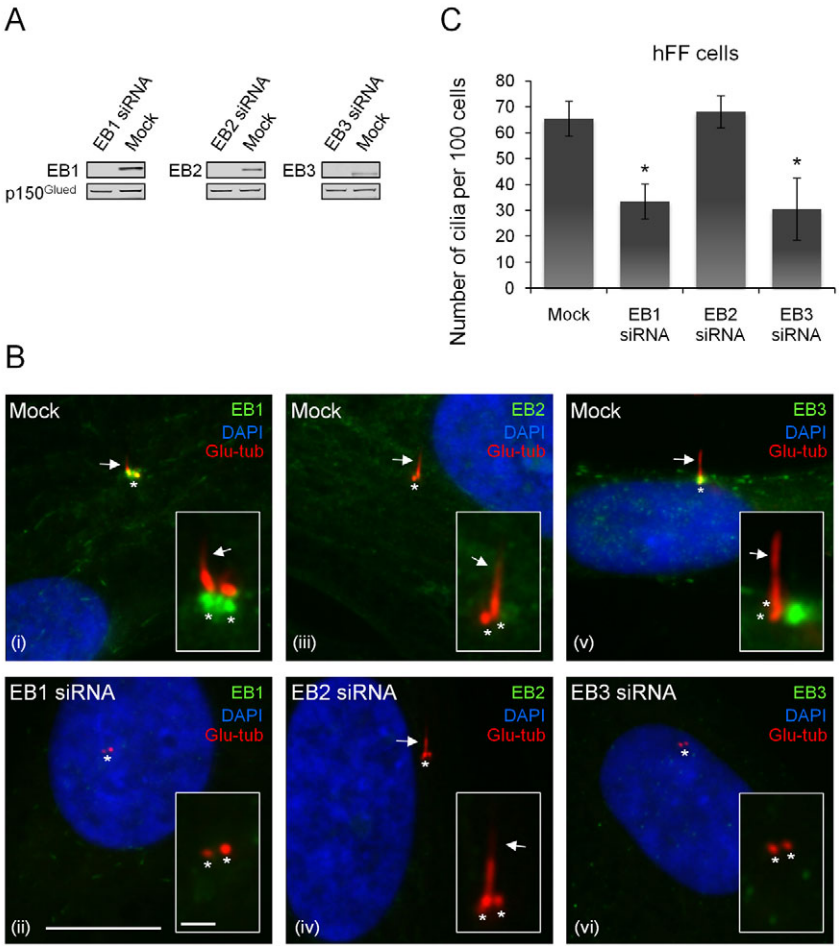

Fig. 1. Depletion of EB1 or EB3, but not EB2, inhibits cilia formation. Human foreskin fibroblasts (hFFs) were treated with mock or EB-specific siRNA, as indicated, grown to confluency and serum starved for 48 hours. (**A**) Western blot analysis of lysates of mock or EB-siRNA-treated cells. Dynactin subunit p150^{Glued} serves as loading control. (**B**) IFM images of methanol-fixed cells stained with Glu-tub antibody (red) and with rat monoclonal EB1, EB2 or EB3 antibodies (green) (Komarova et al., 2005). DNA was stained with DAPI (blue). Arrows indicate primary cilia, asterisks mark centrioles. Insets are enlarged images of the cilium or centriole region (shifted overlays). Scale bars: main panels, 10 μm; insets, 3 μm. (**C**) Quantitative analysis of IFM results. Each column represents the average of three independent experiments with at least 100 cells counted per sample each time; error bars represent standard deviation (s.d.). *, significantly different from mock control (P<0.01). Similar results were obtained in RPE cells (percent ciliated cells were: mock, 66±1%; EB1 siRNA, 30±1%; EB2 siRNA, 66±1%; EB3 siRNA, 34±10%).

EB2 siRNA) and when cilia were stained with antibody against the ciliary membrane marker Arl13B (Caspary et al., 2007) (supplementary material Fig. S1). Importantly, western blot analysis with antibody specifically recognizing retinoblastoma tumor suppressor protein (Rb) phosphorylated at serine residues Ser807 and Ser811 (Knudsen and Wang, 1997) indicated that the siRNA-treated cells were in growth arrest (supplementary material Fig. S2A); and IFM with Ki67 antibody (Gerdes et al., 1984) confirmed this result (supplementary material Fig. S2B). The reduction in ciliation frequency observed upon EB1 or EB3 depletion is, therefore, unlikely to result from cell cycle perturbation.

Expression of dominant-negative EB1 or EB3 inhibits cilia formation

Previous work showed that the C-terminal region of EBs exhibits a dominant-negative effect by disrupting native EB protein dimers and/or by interfering with the association between native EBs and their binding partners (Askham et al., 2002; Etienne-Manneville et al., 2005; Geraldo et al., 2008; Komarova et al., 2009; Schrøder et al., 2007; Wen et al., 2004; Zhou et al., 2004). Specifically, recent evidence indicates that C-terminal EB fragments heterodimerize with endogenous proteins to create 'half dimers' with only one CH domain and, thus, reduced MT affinity (Komarova et al., 2009).

To confirm the siRNA results (Fig. 1), we generated RPE cell lines that stably express GFP-tagged full-length (FL) EB1 or EB3 (GFP-EB1-FL or GFP-EB3-FL, respectively), or GFP-tagged C-terminal (dominant negative) EB1, EB2 or EB3 (GFP-EB1-C, GFP-EB2-C or GFP-EB3-C, respectively) (GFP was at the N-terminus of all EB fragments). We obtained multiple RPE clones expressing GFP-tagged FL or C-terminal EBs and selected several of these for further analysis (Fig. 2A–D). Note that, for GFP-EB1-FL, two different clones with different expression levels of the fusion protein were analysed (clones GFP-EB1-FL1 and GFP-EB1-FL2); the same was the case for GFP-EB2-C (clones GFP-EB2-C1 and GFP-EB2-C2). Quantitative western blot (see Materials and Methods for details) was used to determine the relative molar levels of native and GFP-tagged FL EB1 or EB3 in selected cell lines (Fig. 2F). Since EB antibodies might bind to GFP-EB-C fusions with reduced affinity (e.g. compare the EB1 and GFP blots in Fig. 2A), we did not determine the precise cellular levels of these fusion proteins. However, on the basis of the western blot with GFP antibody, we estimate that all GFP-EB-C fusions analyzed were expressed at a level similar to that of GFP-EB1-FL1 – except GFP-EB2-C2, whose expression levels were considerably higher (Fig. 2A,D). IFM of serum-starved cells using anti-Glu-tub antibody revealed that cultures expressing GFP-EB1-C or GFP-EB3-C had ~50% fewer ciliated cells than cultures expressing GFP, GFP-EB1-FL1, GFP-EB3-FL or GFP-EB2-C (Fig. 2E; for western blot of the GFP-expressing cells, see Fig. 3C). Western blot with antibody against phosphorylated Rb (phospho-Rb antibody) confirmed that cells were in growth arrest (supplementary material Fig. S2C). Since EB1 and EB3 form homodimers and also heterodimerize with each other but not with EB2 (De Groot et al., 2010; Komarova et al., 2009), GFP-EB1-C and GFP-EB3-C are expected to disrupt native EB1–EB3 homo- and heterodimers, but not EB2 homodimers, whereas GFP-EB2-C is expected to affect the EB2 pool only. The above results are, therefore, consistent with the siRNA results (Fig. 1) and suggest that EB1 and EB3, but not EB2, are important for assembly of primary cilia.

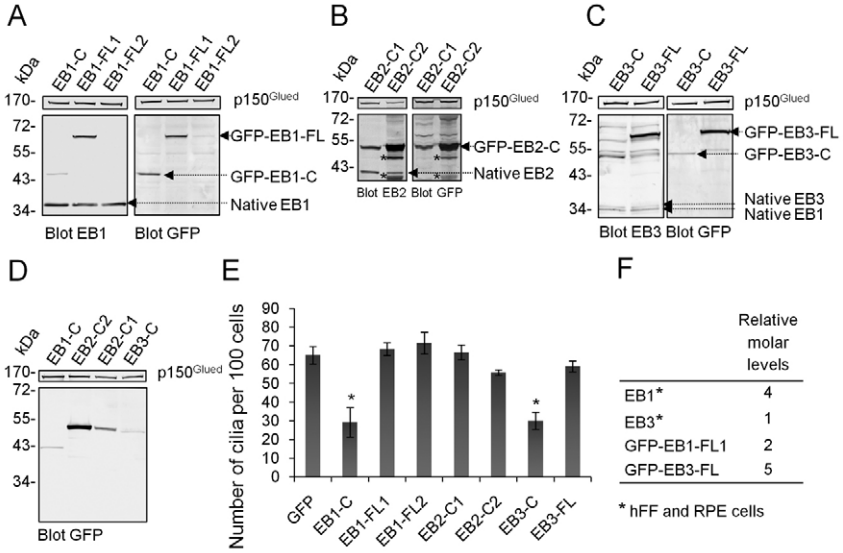

Fig. 2. Expression of dominant-negative EB1 or EB3 inhibits cilia formation in RPE cells. RPE cells stably expressing GFP-tagged full-length (-FL) or C-terminal EB (-C) constructs were grown to confluency and serum starved for 72 hours. (**A**) Western blot analysis of lysates of GFP-EB1-FL (clones 1 and 2) and GFP-EB1-C using EB1, GFP or p150^{Glued} (loading control) antibodies. (**B**,**C**) Similar analysis was performed for cell lines expressing GFP-tagged C-terminal EB2 (B) or GFP-tagged FL or C-terminal EB3 (C). Asterisks in panel B indicate extra bands that are probable degradation or aggregation products resulting from overexpression of the GFP-EB2-C fusion protein. Although the EB3 antibody used in panel C (Komarova et al., 2005) crossreacts with EB1 and three additional bands at ~55–70 kDa, siRNA depletion demonstrated its specificity in IFM analysis (Fig. 1Bv,vi). (**D**) Western blots of RPE cell lines using monoclonal antibody against GFP to compare fusion protein levels. (**E**) Quantification of cilia in the RPE cell lines. A GFP-expressing RPE cell line was used as control (see Fig. 3C for western blot). The analysis was done as in Fig. 1C. Error bars display the s.d. *, significantly different from GFP expressing control (P<0.001). (**F**) Relative molar levels of native or GFP-tagged EB1 or EB3, as determined by quantitative western blot with EB antibodies (see Materials and Methods for details). Molar levels are presented relative to native EB3 levels.

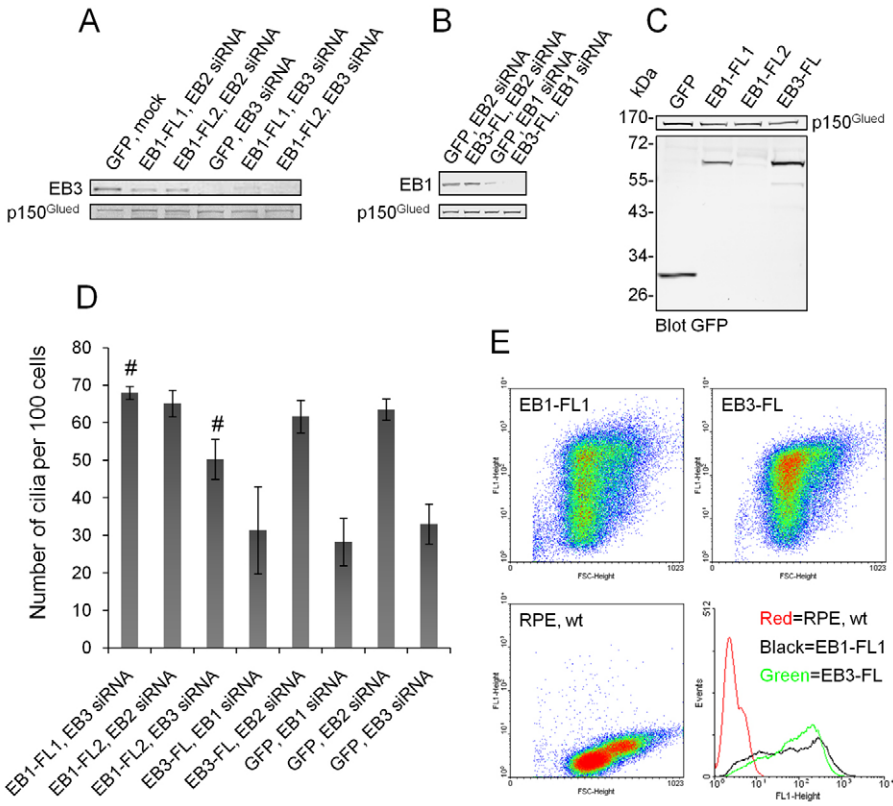

Fig. 3. Expression of GFP-EB1-FL prevents inhibition of cilia formation upon depletion of EB3. RPE cells stably expressing GFP or GFP-tagged EB constructs (Fig. 2) were treated with siRNA, as indicated, grown to confluency and serum starved for 72 hours. (**A**,**B**) Western blots of cell lysates using antibodies as indicated. (**C**) RPE cell lines not treated with siRNA were analyzed by western blot with monoclonal antibody against GFP to compare GFP fusion protein levels. (**D**) Quantification of cilia in cells treated like those shown in A and B. Error bars display the s.d. #, significantly different from GFP-expressing cells treated with EB3 siRNA (GFP, EB3 siRNA) ($P<0.05$). (**E**) FACS analysis of untransfected RPE cells and clones GFP-EB1-FL1 and GFP-EB3-FL showing the fluorescence intensities of GFP. GFP-EB3-FL displays an approximately twofold higher average GFP fluorescence level than GFP-EB1-FL1.

EB3 localizes to the tip of motile cilia in bronchial epithelial cells – EB1 does not

Chlamydomonas contains a simple EB protein, CrEB1, which localizes to the flagellar tip and the proximal end of basal bodies (Pedersen et al., 2003), but ciliary tip localization has not been documented for any mammalian EBs. To address this, we performed IFM analysis by using a variety of different EB1 or EB3 antibodies (Komarova et al., 2005; Stepanova et al., 2003) and confirmed that native EB1 and EB3 localize to the base of primary cilia in RPE and hFF cells (Fig. 1B and data not shown). However, we detected neither EB1 nor EB3 at the ciliary tip in these cells, which is consistent with previous work on EB1 in mouse NIH3T3 cells (Schrøder et al., 2007), although faint staining of cilia was observed in some hFFs labeled with rat monoclonal EB3 antibody (Komarova et al., 2005) (data not shown). Similarly, we did not observe significant enrichment of GFP-EB1-FL or GFP-EB3-FL at the ciliary tip in RPE cells (supplementary material Fig. S3A,B), although both GFP fusions were detected at the basal body and along the length of cilia (supplementary material Fig. S3A,B). The ability of GFP-EB1-FL to localize to cilia contrasts with observations of native EB1, which appears to be absent from cilia, indicating that the GFP tag affects the localization of EB1, consistent with a previous report (Skube et al., 2010).

The apparent absence of native EB1 and/or EB3 at the tip of primary cilia might be owing to differences in axoneme structure or dynamics as compared to motile cilia and flagella, such as those found in *Chlamydomonas*. To investigate this we performed IFM analysis of human bronchial epithelial cells (HBECs) or mature spermatozoa using the same antibodies as for staining of RPE and hFF cells. Interestingly, this analysis detected native EB3, but not EB1, at the tip of motile cilia in HBECs. However, neither EB1 nor EB3 were detected at the flagella tip of mature spermatozoa (Fig. 4 and data not shown). This indicates that the presence of EB3 at the tip of cilia in *Chlamydomonas* and HBECs is not related to the motility of these cilia, but probably reflects higher rates of MT turnover in the axonemes of these cilia compared with primary cilia and mature sperm flagella (see Discussion). The presence of EB3 at the tip of some cilia might promote persistent growth of axonemal MTs. Consistent with this we found that overexpression of GFP-EB3-FL led to cilia elongation in RPE cells (supplementary material Fig. S3C). Although the presence of a GFP tag might affect the function of EB3 within cilia, our results collectively suggest that EB3 is involved in regulating axoneme elongation in certain types of cilium.

Expression of GFP-EB1-FL prevents inhibition of cilia formation upon depletion of EB3

To investigate whether EB1 and EB3 affect ciliogenesis by similar or separate mechanisms, we first tested whether GFP-EB1-FL can substitute for EB3 in ciliogenesis by depleting EB3 or EB2 (control) from RPE clones GFP-EB1-FL1 or GFP-EB1-FL2, respectively, or from GFP-expressing control cells (Fig. 3A–C). Confluent, serum-starved cells were analyzed by IFM with Glu-tub antibody and cilia were quantified. Interestingly, when EB3 was depleted from the GFP-EB1-FL1 cells that contain about twice as many molecules of GFP-EB1-FL as native EB3 (Fig. 2F), no reduction in ciliation frequency was observed compared with EB2-depleted control cells, whereas depletion of EB3 in GFP-expressing cells reduced ciliation frequency – as expected – by 50% (Fig. 3D). Even clone GFP-EB1-FL2, which expresses GFP-EB1-FL at a level that is very low compared with that of the native protein (Fig. 2A), was able to compensate for EB3 depletion to some extent; the

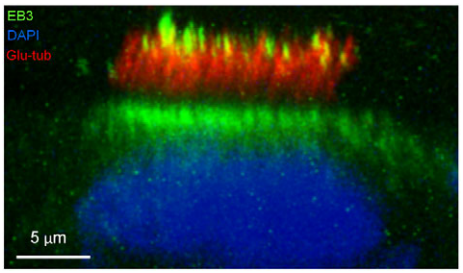

Fig. 4. EB3 localizes to the tip of motile cilia of bronchial epithelial cells. Human bronchial epithelial cells were fixed with cold methanol followed by 4% formaldehyde in PBS. The cells were stained with antibodies against EB3 (green) and acetylated α-tubulin (red) to label cilia; nuclei were visualized with DAPI (blue). The image shows a side view of a single cell. Note the presence of EB3 at the tip as well as the base of cilia.

proportion of ciliated cells in response to EB3 depletion in this clone was ~15% higher than EB3 depletion in a clone that only expressed GFP (Fig. 3D).

Surprisingly, when we tested whether GFP-EB3-FL compensates for EB1, we found this not to be the case. Depletion of EB1 from GFP-EB3-FL cells reduced the frequency of cilia formation by 50%, similar to EB1-depleted GFP-expressing cells (Fig. 3B,D). Fluorescence activated cell sorting (FACS) and western blot with anti-GFP antibody confirmed that GFP-EB1-FL1 is expressed at a lower cellular level than GFP-EB3-FL (Fig. 3C,E), consistent with quantitative western blot analysis performed with anti-EB antibodies (Fig. 2F). Therefore, the most probable explanation of our results is that EB1 has a specific function in ciliogenesis that GFP-EB3-FL is unable to carry out. Alternatively, GFP-EB3-FL might be dysfunctional, but this is unlikely given that it tracks MT plus ends (supplementary material Fig. S3B) and promotes cilia elongation (supplementary material Fig. S3C). Further, we noticed that GFP-EB3-FL can readily substitute for endogenous EB3 in CHO-K1 cells (Komarova et al., 2009).

Ultrastructural defects in cells that lack EB1 or EB3

To address the mechanisms by which EBs affect ciliogenesis, we analyzed siRNA-treated, serum-starved hFF cells using serial thin sectioning and transmission electron microscopy (TEM). Analysis of mock-transfected control cells revealed features typical of cells with primary cilia (Albrecht-Buehler and Bushnell, 1980; Molla-Herman et al., 2010; Sorokin, 1962), including basal bodies (bb) with associated transition fibers (tf) and subdistal appendages (sda), and a ciliary shaft embedded within a membrane pocket (Fig. 5A). Further, the mock-transfected control cells displayed a highly organized radial MT array emanating from the subdistal appendages of the basal body (Fig. 5B,C). By contrast, in EB1-depleted cells the MT array anchored at the basal body appeared highly disorganized and cells with abnormally short cilia stumps were seen (Fig. 5D–I). In the EB3-depleted cells the MT array surrounding the basal body appeared similarly disorganized (e.g. Fig. 6E,H), and many EB3-depleted cells contained stumpy cilia that displayed vesicle accumulation within (Fig. 6B,C,E,F) or around (Fig. 6H–J) the cilia compartment, and/or exhibited tubular extensions of the cilium pit (Fig. 6G). Vesicle accumulation was also observed in the vicinity of basal bodies of EB1-depleted cells (Fig. 5D–F). The transition fibers and subdistal appendages appeared normal in the EB1-depleted (Fig. 5D–I) and EB3-depleted (Fig. 6K,L) cells, but these cells occasionally displayed centrioles with subdistal appendages that were placed one above the other on a single centriole (Fig. 5I and Fig. 6N) or centrioles with less than nine subdistal appendages attached in a single plane to the centriole wall (Fig. 6L). These observations probably reflect occasional variations in subdistal appendage number and placement, because similar observations were reported in NIH3T3 cells (Albrecht-Buehler and Bushnell, 1980) and human lymphoblasts (Paintrand et al., 1992). Thus, EB1- and EB3-depleted cells contain stumpy cilia, a disorganized MT array surrounding the basal body, and accumulation of vesicles near or within cilia stumps. We did not observe significant Golgi disintegration upon siRNA depletion of EB1 or EB3, as revealed by IFM with GMAP-210 antibody (data not shown), consistent with previous reports (Askham et al., 2002; Watson and Stephens, 2006). This suggests that any effect of EB inactivation on cilia-related vesicle transport is not due to general defects in Golgi trafficking.

Defective MT minus-end anchoring in cells that lack EB1 or EB3

Since our TEM analysis (Figs 5, 6) indicated that the MT array surrounding the basal body is disorganized in cells that lack EB1 or EB3, we next tested whether MT minus-end anchoring is defective in these cells. Previous work implicated EB1 in MT minus-end anchoring at the centrosome (Askham et al., 2002; Louie et al., 2004; Yan et al., 2006), but a role for EB3 in centrosomal MT minus-end anchoring was not investigated. To address this we used CHO-K1 cells, which have been used extensively to study the MT dynamics (Komarova et al., 2002; Komarova et al., 2005; Komarova et al., 2009). Cells were transfected with previously described pSuper-based short hairpin (sh) RNA vectors to knockdown EB1 or EB3 (Komarova et al., 2005). The consequent effect on MT minus-end anchoring at the centrosome was assessed by estimating the frequency of MT releases from the observed shortening of minus ends on the subtracted images of the cells following microinjection with Cy3-labeled tubulin (Vorobjev et al., 1999). Knockdown of either EB1 or EB3 caused an approximately threefold increase in the frequency of MT releases compared with control cells (Table 1). Expression of the dominant-negative EB1 mutant EB1-CΔAc (Komarova et al., 2009) had an effect comparable to that of EB1 or EB3 depletion; the frequency of MT releases was approximately twofold higher after overnight expression and similar to that in control cells 2–3 hours after expression of the mutant (Table 1). These results indicate that both EB1 and EB3 are important for MT anchoring at the centrosome.

EB1 and EB3 interact with proteins that are implicated in centrosomal MT minus-end anchoring and ciliary vesicle transport

To further investigate the mechanisms by which EBs promote ciliogenesis, we used GST pull-down assays and mass spectrometry (Grigoriev et al., 2008) to identify potential EB binding partners in ciliated RPE cells. Interestingly, in addition to identifying well-characterized EB partners, such as $p150^{Glued}$ and CDK5RAP2 (also known as Cep215) (Akhmanova and Steinmetz, 2008; Fong et al., 2009), we identified several new potential EB interactors with known cilium- or centrosome-related functions (Table 2; supplementary material Fig. S4). Most prominent among these was PCM1 (Table 2), a pericentriolar satellite protein involved in MT-based trafficking to cilia and

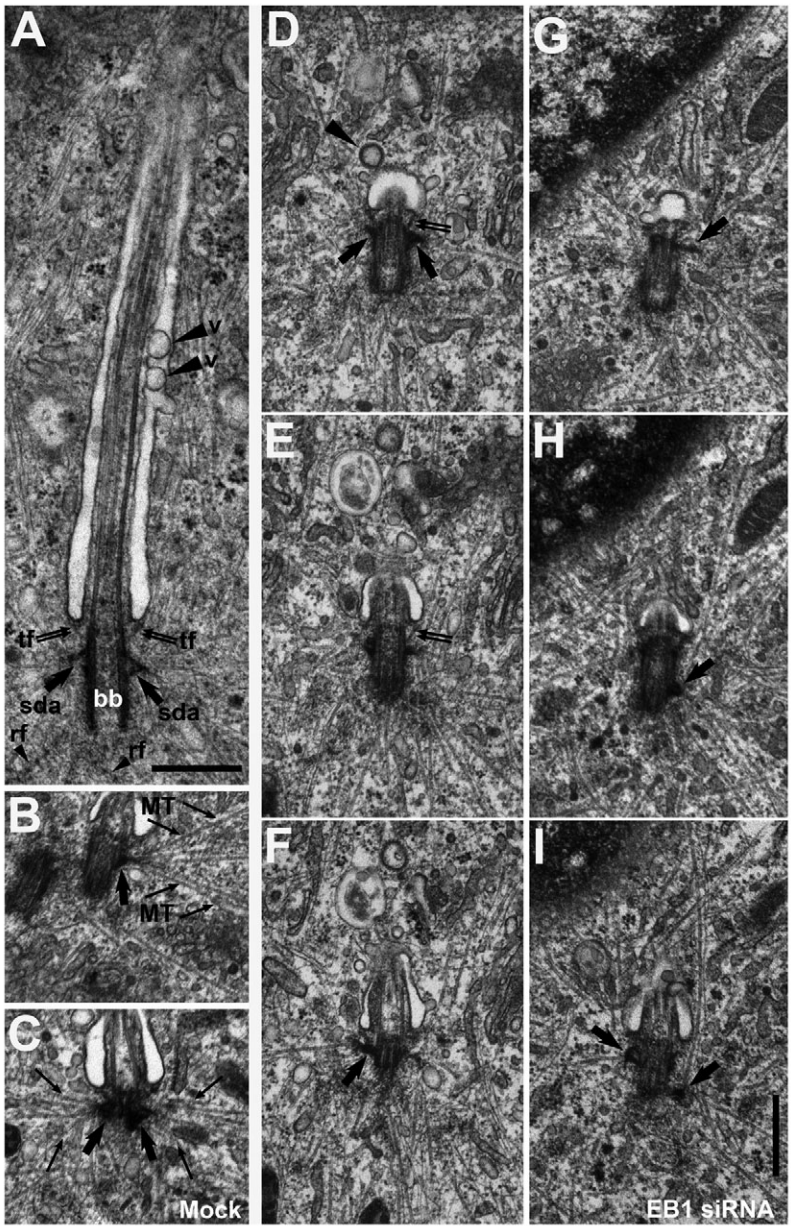

Fig. 5. Ultrastructural analysis of hFF cells treated with mock or EB1-specific siRNA. TEM analysis of growth-arrested control (mock; **A–C**) or EB1-depleted (**D–I**) hFF cells. (A) Longitudinal section of a basal body (bb) and attached primary cilium. Transition fibers (tf; thin double arrows), subdistal appendages (sda; thick arrows) and rootlet filaments (rf; small arrowheads) are visible. In the cilium pit two vesicles (v; large arrowheads) are present. (B,C) Grazing longitudinal sections of basal bodies. Microtubules (MT; thin arrows) radiating in a fan-like pattern from the subdistal appendages (thick arrows) are seen. (D,F) Consecutive longitudinal serial sections of a basal body bearing a stumpy cilium. Subdistal appendages (D–F; thick arrows) and transition fibers (D,E; thin double arrows) can be seen. In D, a coated vesicle constricting from the cilium-pit is visible (large arrowhead). (G–I) Consecutive longitudinal serial sections of a basal body with attached stumpy cilium. Three subdistal appendages can be seen, one of which is attached to the centriole in a more median to proximal position (H,I; thick arrows at the right side of the centriole) than the other two (G,I; thick arrows). Scale bars: A, 500 nm; I, 500 nm (applies to B–I).

centrosomes (Kubo et al., 1999). Previous work has shown that PCM1 interacts with BBS proteins, p150^{Glued}, Cep290 and Rab8 to promote vesicular trafficking to cilia (Dammermann and Merdes, 2002; Kim et al., 2008; Kim et al., 2004; Nachury et al., 2007). Since EBs bind directly to p150^{Glued} (Akhmanova and Steinmetz, 2008), they might interact with PCM1 (and Cep290) through this protein. Immunoprecipitation of ciliated RPE cell lysate using p150^{Glued} antibody co-precipitated PCM1, Cep290, EB1 and EB3 (supplementary material Fig. S4C). Further, immunoprecipitation with EB1 antibody also co-precipitated PCM1 and p150^{Glued} (data not shown). These results indicate that EB1 and EB3 interact, at least indirectly, with PCM1.

We addressed the importance of EBs in the localization of PCM1 and Cep290 by using IFM for our stable RPE cell lines (Fig. 2) or siRNA-treated hFFs. By using this approach we did not detect any gross alterations in the sub cellular localization of PCM1 or Cep290 upon inactivation of EB. Similarly, we found that localization of ninein, CEP250 (also known as CNAP1), γ tubulin and CEP170 was not substantially altered upon inactivation of EB1 or EB3 (data not shown). However, subtle alterations in the sub-cellular localization of these proteins cannot be excluded.

Partial depletion of p150^{Glued} inhibits ciliogenesis in NIH3T3 cells

In a previous study we have addressed the importance of the interaction between EB1 and p150^{Glued} for the assembly of primary cilia in NIH3T3 cells, by using a variety of mutant dominant-negative EB1-GFP constructs. On the basis of the results obtained with these constructs, we concluded that interaction between EB1 and p150^{Glued} is important for ciliogenesis (Schrøder et al., 2007). However, a caveat with this conclusion is that all the EB1 fusions used in (Schrøder et al., 2007) had the GFP-tag at the C-terminus (Wen et al., 2004), thereby preventing access to the C-terminal

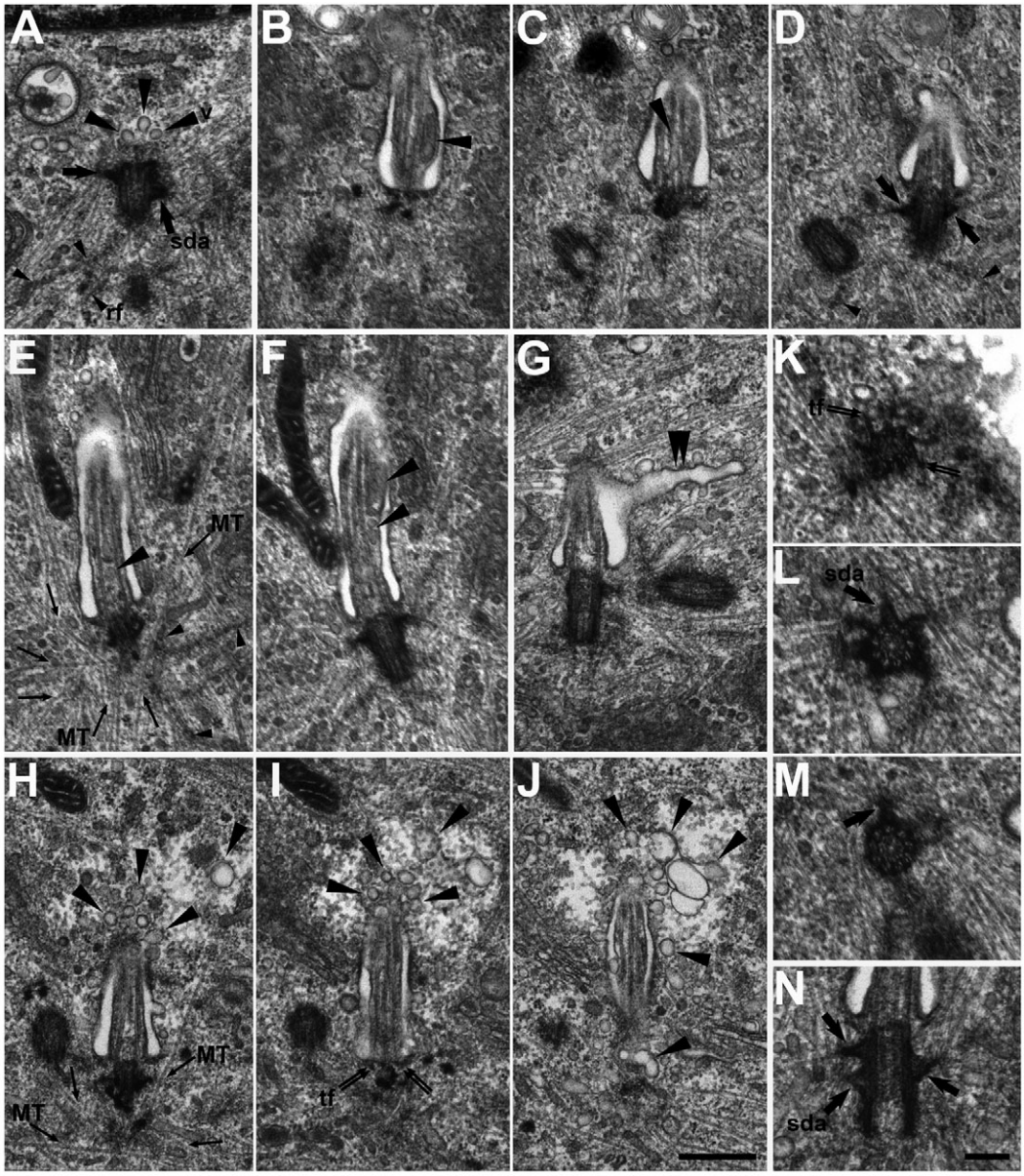

Fig. 6. Ultrastructural defects in cells lacking EB3. TEM analysis of growth-arrested, EB3-depleted hFF cells. (**A**) Longitudinal section of a mother centriole with subdistal appendages (sda; thick arrow). At the distal end of the centriole three vesicles are visible (v; large arrowheads). Rootlet filaments (rf) are labeled (small arrowheads). (**B**–**D**) Consecutive serial longitudinal sections of a basal body with a stumpy cilium. Vesicles (large arrowheads) are visible within the cilium. In D, the oblique sectioned daughter centriole, subdistal appendages (thick arrows) attached to the basal body and rootlet filaments (small arrowheads) can be seen. (**E**,**F**) Consecutive serial longitudinal sections of a basal body with stumpy cilium. Vesicles (large arrowheads) are accumulated within the cilium. (**G**) Longitudinal section of a basal body bearing a stumpy cilium. The cilium pit shows a long, tubular extension (large double arrowheads). The oblique sectioned daughter centriole is visible to the right. (**H**–**J**) Consecutive longitudinal serial sections of a basal body with stumpy cilium. The cytoplasmic area around the tip of the cilium looks distorted and many vesicles (large arrowheads) are present. In J, vesicles (large arrowhead at the bottom of the panel) can be seen, which are localized in the region of the attachment site between the transition fibers (tf; thin double arrows in I) and the membrane of the cilium pit. (**K**–**M**) Consecutive serial cross sections of a mother centriole. The transition fibers (tf; thin double arrows) attached to the distal end of the centriole are clearly visible (K). At least six subdistal appendages are associated with the centriole in a subdistal position (L, sda; thick arrow); one additional subdistal appendage is associated with the centriole in a more median to proximal position (M, thick arrow). (**N**) Longitudinal section of a basal body. At the left side of the centriole two subdistal appendages (sda; thick arrows) are associated, above each other, with the centriole; at the right side only one subdistal appendage (thick arrow) is present. Scale bars: J, 500 nm (applies to A-J); N, 200 nm (applies to K–N).

acidic tail of EB1 that is known to be essential for binding to $p150^{Glued}$ (Akhmanova and Steinmetz, 2008). Therefore, to directly address its role in ciliogenesis, we partially depleted $p150^{Glued}$ from NIH3T3 cells by using siRNA, and found that cells depleted for $p150^{Glued}$, indeed, produced cilia with much lower frequency than control cells (supplementary material Fig. S5).

EB3 affects the formation of centriole-associated rootlet filaments

During TEM analysis, we noticed that cells depleted for EB3 display abnormally long rootlet filaments at the proximal end of centrioles (Fig. 7A–F). To investigate this further we used IFM and anti-rootletin antibody to analyze EB3-depleted hFFs (Bahe et al.,

Table 1. Frequency of microtubule release from the centrosome in CHO-K1 cells upon EB depletion or inactivation

	Number of cells observed	Release frequency in minutes^{-1}
Control cells*	11	1.0±0.5
Expression of shRNA		
EB1	5	3.4 (79 microtubules in 23.3 minutes)
EB3	5	3.4 (102 microtubules in 29.7 minutes)
Expression of EB1-CΔAc		
2–3 hours	9	0.7 (40 microtubules in 59.4 minutes)
Overnight	7	2 (82 microtubules in 42.7 minutes)

*Data from Komarova et al. (Komarova et al., 2002) included for comparison.

2005). Our analysis confirmed that EB3-depleted cells contain centrioles with a more extended rootlet system than mock-transfected or EB1-depleted cells (Fig. 7G,I). IFM analysis of our stable transfected RPE cell lines (Fig. 2) revealed a similar, abnormal, rootletin staining in cells expressing GFP-EB1-C or GFP-EB3-C, but not in cells expressing GFP, GFP-EB1-FL1 or GFP-EB3-FL (Fig. 7H,J and data not shown). Since C-terminal EB1 and EB3 fragments both interfere with the formation of EB3 dimers (De Groot et al., 2010; Komarova et al., 2009), these results reinforce the notion that EB3 affects the formation of rootlet filaments. Rootletin interacts with CEP250 and β-catenin, which are involved in regulating centrosome cohesion through a complex mechanism that involves Nek2, Axin2 (also known as conductin) and Wnt signaling (Bahe et al., 2005; Bahmanyar et al., 2008; Hadjihannas et al., 2010). We found that staining of phosphorylated β-catenin at the centrosome – similar to that of rootletin – was perturbed in cells that express GFP-EB1-C or GFP-EB3-C, whereas CEP250 localized normally in all cell lines examined (data not shown). We also tested whether EBs affect centrosome cohesion by measuring inter-centriolar distances (assessed by IFM using anti-Glu-tub antibody), but found no evidence of centrosome splitting in EB1- or EB3-depleted cells under the conditions used here (n=3 with at least 50 cells analyzed per sample). Finally, we tested whether GFP-EB1-FL can rescue the rootlet phenotype of EB3-depleted cells. We found that it can not (data not shown), which suggests that the ability to affect rootlet filament formation is unique for EB3. Consistent with a role for EB3 in regulating rootlet filament formation, we identified rootletin as a potential EB3 partner in our pull-down assays (Table 2).

Discussion

Using various approaches we have shown that EB1 and EB3 are required for assembly of primary cilia in cultured cells, and that both are required for MT minus-end anchoring at the centrosome. Overexpression of truncated CAP350 leads to removal of EB1 from the centrosome but not from MT plus ends (Yan et al., 2006) and on the basis of this result we previously suggested that EB1 affects ciliogenesis at the level of the basal body (Schrøder et al., 2007). However, the CAP350 fragment described by Schrøder et al. (Schrøder et al., 2007) also removes FGFR1OP, and potentially additional proteins, from centrosomes (Yan et al., 2006), thus complicating the interpretation of our initial results. In CHO-K1 cells, catastrophe suppression is the main function of EBs at MT plus ends and, whereas single knockdown of EB1 or EB3 had little effect on MT growth, their simultaneous depletion severely impaired persistent MT growth by increasing the occurence of MT catastrophes (Komarova et al., 2009). Our results from EB1 or EB3 single knockdown, therefore strongly suggest that EB1 and/or EB3, indeed, affect ciliogenesis through effects at the basal body or cilium, and not through alterations of cytoplasmic MT plus-end dynamics. Further support of this idea is the fact that GFP-EB1-FL can substitute for EB3 in ciliogenesis even though MT plus ends are poorly tracked by GFP-EB1-FL (supplementary material Fig. S3A). By contrast, GFP-EB3-FL cannot compensate for lack

Table 2. Identification of EB binding partners by using GST pull-down assay and mass spectrometry*

		Mascot score			Unique peptides / total peptides		
Identified proteins	IPI accession	EB1	EB2	EB3	EB1	EB2	EB3
APC	IPI00012391	71		57	2/2		2/2
CDK5RAP2 (Cep215)	IPI00329038	92	42		3/3	2/2	
CLASP 1	IPI00396279	1528	942	1816	31/76	21/26	36/95
Clip-170	IPI00217113	3854	2023	4290	63/226	44/86	68/395
Dynactin 1 (p150^{Glued})	IPI00029485	3781	1168	3338	51/278	26/40	50/251
MCAK (Kif2C)	IPI00290435	573		616	12/22		12/28
STIM1	IPI00299063	1387		410	23/74		10/16
Centlein	IPI00657839			55			2/3
Cep170	IPI00186194	252	288		6/9	8/10	
Cep250 (C-Nap1)	IPI00160622	41			1/51		
Cep290	IPI00784201	40			1/18		
Ninein	IPI00441959	413	105	80	12/16	2/8	4/5
PCM1	IPI00006213	357	45	278	9/10	2/3	8/10
Rootletin	IPI00456492			87			4/4
SMC1A	IPI00291939			59			2/4

*Proteins above the line are previously characterized EB binding partners, whereas proteins listed below this line represent new potential EB interactors. Additional EB partners identified in this analysis will be described elsewhere.

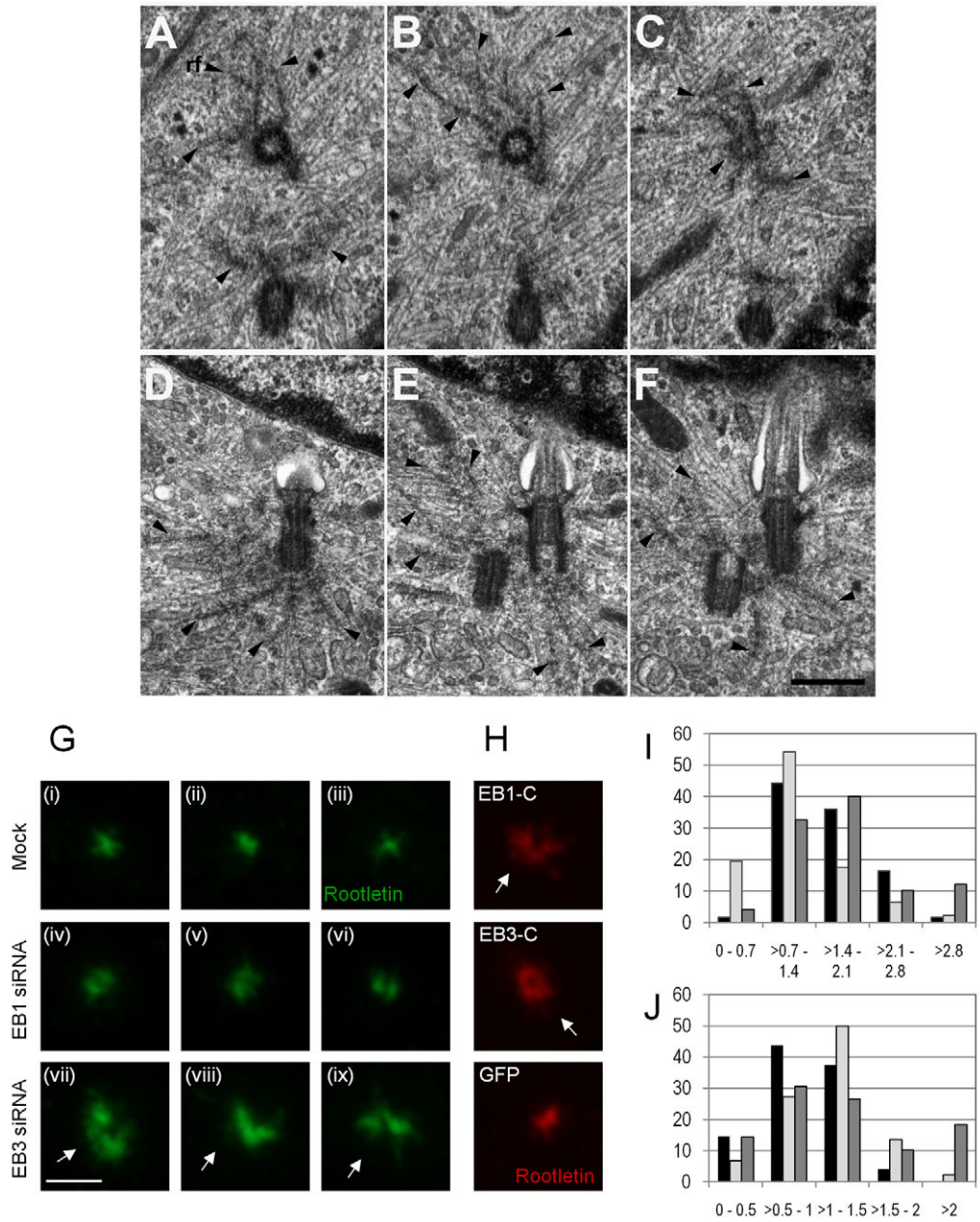

Fig. 7. Cells lacking EB3 contain abnormally long rootlet filaments. (**A–F**) TEM analysis of growth-arrested, EB3-depleted hFFs. (A–C) Consecutive serial cross sections of a centriole displaying an elaborate and extended rootlet filament (rf) system (small arrowheads). The second centriole is sectioned in an oblique angle. (D–F) Consecutive longitudinal serial sections of both centrioles with the basal body bearing a stumpy cilium. Both centrioles display an elaborate system of rootlet filaments (small arrowheads) attached to their proximal end. Scale bar: 500 nm. (**G**) IFM of siRNA-treated, serum-starved hFFs stained with anti-rootletin antibody (Bahe et al., 2005). Abnormally long rootlets are seen in EB3-depleted cells (arrows in vii-ix). (**H**) Different RPE cell lines (see Fig. 2) analyzed by IFM with rootletin antibody. Unfocused rootletin staining (arrows) is seen in cell lines expressing GFP-EB1-C or GFP-EB3-C. Similar dispersal of phosphorylated β-catenin staining was observed in the same cell lines (data not shown). Scale bar: 3 μm (applies to G and H). (**I**,**J**) Quantification of the results shown in G and H, respectively. The *x*-axis depicts area of rootletin staining in μm^2, whereas the *y*-axis indicates percent of cells (44–61 cells analyzed per sample). In I, mock-, EB1 siRNA- and EB3 siRNA-treated cells are represented by black, light gray and dark gray columns, respectively. In J, GFP-, GFP-EB1-C and GFP-EB3-C expressing cells are represented by black, light gray and dark gray columns, respectively. Note that depletion of EB3 (I) or expression of GFP-EB1-C or GFP-EB3-C (J) causes an increase in the area of rootletin staining in many cells.

of EB1, although it was expressed at similar levels. A likely explanation for this result is that EB3 homodimers appear less stable than EB1 homodimers or EB1-EB3 heterodimers, and might, therefore, have different functional properties than EB1-containing dimers (De Groot et al., 2010; Komarova et al., 2009). In support of this we found that EB3 localizes to the tip of motile cilia of HBECs and affects the formation of centriole-associated rootlet filaments, whereas EB1 does not. Although we barely detected EB3 in primary cilia of hFF and RPE cells, a recent proteomics study of isolated mouse photoreceptors identified EB3 in the outer

segment (a modified primary cilium) and EB1 in the inner segment (Liu et al., 2007), indicating that EB3 also localizes to some types of non-motile cilium. By contrast, we found that EB3 appears to be absent from flagella of mature spermatozoa. Such flagella are known to be devoid of intraflagellar transport proteins (J. San Agustin, G. Pazour and G. B. Witman, unpublished data) and are, therefore, presumably not undergoing axonemal MT turnover (Marshall and Rosenbaum, 2001). Hence, localization of EB3 in cilia tips is likely to be confined to cilia with axonemal MTs that are undergoing tip turnover. Since EBs suppress MT catastrophes in CHO-K1 cells (Komarova et al., 2009), *Xenopus* extracts (Tirnauer et al., 2002) and fission yeast (Busch and Brunner, 2004) EB3 might promote cilia stabilization by counteracting proteins that destabilize axonemal MTs. This might occur by direct association of EB3 with axonemal MT lattices (Sandblad et al., 2006; Vitre et al., 2008), which, in turn, might interfere with the binding of destabilizing factors to axonemes. EB3 interacts with the MT depolymerizing kinesin-13 MCAK (Lee et al., 2008). Kinesin-13 family proteins have been implicated in cilium disassembly in protists (Blaineau et al., 2007; Dawson et al., 2007; Piao et al., 2009), and EB3 might, therefore, stabilize the axoneme by counteracting such proteins.

Since inactivation of either EB1 or EB3 has similar effects on MT anchoring and ciliogenesis, these processes are likely to be mediated by EB1 homodimers and EB1–EB3 heterodimers. In mammalian cells the subdistal appendages of the mother centriole are involved in MT minus-end anchoring (Bornens, 2002; Piel et al., 2000) (see also Fig. 5B,C) and high resolution IFM indicated that EB1 localizes close to these appendages (Louie et al., 2004). Ninein and Cep170 – which were both identified as potential EB1 binding partners in our pull-down analysis (Table 2) – localize to the subdistal appendages (Guarguaglini et al., 2005; Mogensen et al., 2000). Furthermore, immunogold EM studies in *Chlamydomonas reinhardtii* showed that EB1 localizes to the proximal part of basal bodies, close to the site where rootlet MTs are linked to the MT triplets of the basal body (Pedersen et al., 2003) by an array of morphologically distinct fibers (Geimer and Melkonian, 2004). These observations are consistent with a role for EBs in MT minus-end anchoring at the subdistal appendages.

The apparent absence of native EB1 in cilia indicates that EB1-containing dimers are unlikely to directly participate in the stabilization of the the cilia axoneme, but that they presumably mediate ciliogenesis through their MT minus-end anchoring activity – similar to ninein which was shown to be important for ciliogenesis in RPE cells (Graser et al., 2007). MT minus-end anchoring probably promotes dynein-mediated trafficking of ciliary precursors to the ciliary base. Evidence highlighting the importance of such trafficking in the assembly and maintenance of cilia is rapidly accumulating, and multiple proteins involved in this process have been identified (Nachury et al., 2010; Pazour and Bloodgood, 2008). For example, PCM1 is thought to function with dynactin, BBS proteins, and Rab11 and Rabin8 to promote dynein-mediated transport of vesicles that carry ciliary proteins from pericentriolar satellites towards the cilium base where the vesicles are exocytosed (Dammermann and Merdes, 2002; Kim et al., 2008; Kim et al., 2004; Kubo et al., 1999; Nachury et al., 2007; Westlake et al., 2011). If MT minus-end anchoring at the basal body is defective (e.g. upon inactivation of EB1 or EB3), such vesicles might be targeted to the wrong place and ciliogenesis would be impaired. Although we did not observe any gross mislocalization of PCM1 or Cep290 upon inactivation of EB1 or EB3, this could be owing to the limited resolution of the IFM procedure. In our TEM analyses, we frequently observed accumulation of vesicles near cilium stumps of EB1- or EB3-depleted cells (e.g. Fig. 5D–F and Fig. 6H–J), consistent with defective vesicle trafficking. It will be interesting to further investigate the role of EBs in vesicular trafficking to cilia in live cells, e.g. by using fluorescently tagged Rab8.

The extended rootlet filaments observed upon EB3 depletion are similar to those observed upon depletion of CEP250, which interacts with rootletin and may provide a docking site for rootlet filaments at the proximal end of centrioles (Bahe et al., 2005). CEP250 is required for tethering Axin2 to centrosomes, and conductin in turn regulates centrosome cohesion by altering the phosphorylation status of centrosomal β-catenin (Hadjihannas et al., 2010). EB3 might be part of a centrosomal CEP250–rootletin–conductin–phosphorylated–β-catenin complex involved in regulating the association of rootlets with the centriole wall. Consistent with this idea, we identified rootletin as a potential EB3 partner in our pull-down analysis (Table 2). Neither rootletin nor CEP250 are required for ciliogenesis (Graser et al., 2007; Yang et al., 2005), but studies of a rootletin knockout mouse indicated a role for rootletin in long-term stability of cilia and in orientation of centrioles in photoreceptors (Yang et al., 2005). It is, therefore, possible that the effect of EB3 on rootlet filaments influences cilia stability and/or centriole orientation. This may be particularly relevant in multiciliated epithelia where EB3 is strongly expressed (www.proteinatlas.org) and where appropriate orientation of basal bodies is crucial in the regulation of cilium-mediated liquid flow and planar cell polarity (Guirao et al., 2010; Hashimoto et al., 2010; Mirzadeh et al., 2010). Finally, although the lack of ciliary rootlets causes a relatively mild phenotype in mice (Yang et al., 2005), the presence of rootlets in distorted conformation (e.g. in the absence of EB3) could have a more severe effect.

Materials and Methods

Molecular biology

Plasmid EB1-CΔAc and pSuper-based shRNA constructs for knockdown of EB1 or EB3 in CHO-K1 cells have been described previously (Komarova et al., 2005; Komarova et al., 2009). GFP-EB3-FL and GFP-EB2-FL plasmid constructs were generously provided by Ewan E. Morrison (University of Leeds, UK). These constructs served as templates in PCR-amplification of human EB2-C (residues 159–327) and EB3-C (residues 116–281) using the Herculase Enhanced DNA Polymerase protocol provided by Stratagene and appropriate primers (sequences available upon request). For cloning of human EB1-FL and EB1-C (residues 165–268) mRNA was extracted from hFF cells using the RNeasy protect mini kit (Qiagen), and cDNA was amplified by reverse transcription (RT) PCR using SuperScript II Reverse Transcriptase (Invitrogen). All PCR products were ligated into pEGFP-C1 (Clontech) after digestion with appropriate restriction enzymes, and the ligated plasmids were transformed into competent *E. coli* DH10α cells using standard procedures. Plasmids were isolated from bacterial colonies using standard procedures and plasmids were sequenced (Eurofins MWG Operon, Germany).

Cell cultures

Human foreskin fibroblasts (hFFs; kind gift from Klaus Yding Andersen, Rigshospitalet, Denmark) were grown at 37°C, 5% CO_2, 95% humidity in Iscove's modified Dulbecco's medium (IMDM; Gibco) supplemented with 10% heat-inactivated fetal calf serum (FBS; Gibco) and 10 ml/l penicillin-streptomycin (Gibco). The hFF cultures were passaged every 6–7 days by trypsination (0.5%) and only passages 5–20 were used for experiments. The RPE cells used (lab stock) are derived from the immortalized hTERT RPE-1 cell line, and were grown in 45% Dulbecco´s Modified Eagle's Medium (DMEM; Sigma) and 45% F-12 (Ham; Sigma) with 10% FBS and 10 ml/l penicillin-streptomycin; cultures were passaged every 3–4 days. Stable RPE cell lines were selected by supplementing the medium with 0.5 mg/ml G418 (Gibco). Previous work described culture conditions for CHO-K1 (Komarova et al., 2002) and NIH3T3 cells (Schneider et al., 2005; Schrøder et al., 2007). Subcultures of primary human bronchial epithelial cells (HBECs were obtained from resected normal lung tissue (obtained from Pieter Hiemstra, LUMC Leiden). HBEC were isolated essentially as previously described and allowed to differentiate

Table 3. Antibodies used for immunofluorescence microscopy and western blotting

Antigen	Host organism	Manufacturer	Dilution for WB	Dilution for IFM
Acetylated α-tubulin	Mouse (MAb)	Sigma	–	1:200
Arl13B	Rabbit (PAb)	(Caspary et al., 2007)	–	1:500
C-Nap1 (Cep250)	Rabbit (PAb)	ProteinTech Group	1:800	1:100
Cep170	Rabbit (PAb)	Abcam	1:500	1:200
Cep290	Rabbit (PAb)	Abcam	1:2000	1:500
EB1	Rat (MAb)	Absea (clone KT51)	1:1000	1:200
EB2	Rat (MAb)	Absea (clone KT52)	1:200	1:200
EB3	Rat (MAb)	Absea (clone KT36)	1:200	1:200
EB3	Rat (MAb)	Absea (clone KT53)	1:200	–
GFP	Rabbit (PAb)	Invitrogen	1:1000	–
GFP	Mouse (MAb)	Abcam	1:1000	–
Glu-tub	Rabbit (PAb)	Abcam	1:1000	1:500
GMAP-210	Mouse (MAb)	BD Transduction Laboratories	–	1:500
Ki67	Rabbit (PAb)	Abcam	–	1:500
Ninein	Rabbit (PAb)	Abcam	1:500	1:500
p150^{Glued}	Mouse (MAb)	BD Transduction Laboratories	1:2000	1:1000
PCM1	Rabbit (PAb)	Abcam	1:2000	1:400
Phospho-β-catenin (Ser33, Ser37, Thr41)	Rabbit (PAb)	Cell Signaling Technology	1:1000	1:1000
Phospho-Rb (Ser807, Ser811)	Rabbit (PAb)	Cell Signaling Technology	1:1000	–
Rootletin	Rabbit (PAb)	(Bahe et al., 2005)	1:1000	1:1000
α-tubulin	Mouse (MAb)	Sigma	1:2000	–
γ-tubulin	Rabbit (PAb)	Sigma	–	1:500

WB, western blotting; IFM, immunofluorescence microscopy.

in air-liquid interface (ALI) cultures (van Wetering et al., 2007). Briefly, HBEC were expanded in keratinocyte serum-free medium (KSFM; Invitrogen, Paisley, UK) supplemented with 0.2 ng/ml EGF (Invitrogen), 25 µg/ml bovine pituitary extract (Invitrogen), 1 µM isoproterenol, 20 U/ml penicillin, 20 µg/ml streptomycin. The cells were then seeded at 1.5×10^5 cells/cm^2 in DMEM/BEGM (1:1) medium with supplements (Bulletkit; Lonza, Breda, The Netherlands) on 24-well transwell inserts (0.4 µm pore size, 6 mm diameter; Corning Incorporated, Schiphol-Rijk, The Netherlands). Transwell inserts were pre-coated with 10 µg/ml bovine fibronectin (Sigma, Zwijndrecht, The Netherlands), 30 µg/ml Purecol (Inamed, Fremont, CA, USA), and 10 µg/ml bovine serum albumin. Upon confluence, apical medium was removed and basal medium replaced with DMEM/BEGM medium supplemented with 10 nM retinoic acid (Sigma). When necessary, cells were allowed to differentiate for 2 weeks and basal medium was refreshed and apical mucus was washed off every other day.

Transfection and selection of stable cell lines

Specific cell types were cultured as described above. For CHO-K1 cells, transfection and microinjection procedures were as described (Komarova et al., 2005; Komarova et al., 2009). For the remaining cell types, procedures were as follows. All siRNA experiments were performed in 6×9.6 cm² multiwell plates (Greiner Bio One) and for IFM analysis sterile glass cover slips were placed in the wells before adding the cells. For siRNA transfection of RPE cells ca. 3×10^4 cells/cm^2 were plated per well the day prior to transfection. One hour before transfection, growth medium was replaced with medium without serum and penicillin-streptomycin. The cells were transfected with 100 nM siRNA specifically targeting EB1, EB2 or EB3 (ON-TARGET*plus* siRNA Reagents, Dharmacon) or 100 nM control siRNA (5′-UAAUGUAUUGGAACGCAUATT-3′; Eurofins MWG Operon, Germany) using 5 µl of DharmafectDuo (Dharmacon) per well, and serum (10% final volume) was added to the cultures 1 hour after transfection. On day three, when the cells had reached confluency they were serum starved for 72 hours. For analysis of cells in interphase, cells were grown to ~70% confluency and serum starvation was omitted before analysis. Transfection of hFFs was performed in a similar manner except that 1×10^4 cells/cm^2 were plated the day prior to transfection. The following day, cells had reached ~90% confluency and were serum starved for 48 hours. NIH3T3 cells were transfected at a confluency of ~40–50% with 50 nM or 100 nM siRNA specifically targeting p150^{Glued} (ON-TARGET*plus* siRNA Reagents, Dharmacon) or 100 nM control siRNA (see above) using 5 µl Lipofectamine 2000 (Invitrogen) per 100 nM siRNA. When cells were ~90% confluent the day after transfection, they were serum starved for 24 hours. For generation of RPE cells stably expressing GFP fusion protein, the cells were plated into 94×16 mm CELLSTAR tissue culture dishes (Greiner Bio One) the day before transfecting with 5 µg plasmid DNA (see above) using 20 µl of DharmafectDuo per dish. The following day, before adding selection medium (growth medium containing G418), transfected cells were replated into new dishes to a cell density of ~1×10^4 cells/cm^2. After about 10–12 days of selection replacing the media every 3–4 day the colonies were picked following treatment with PBS containing 10 mM EDTA. FACS analysis was performed using Becton-Dickinson FACS Aria.

Antibodies

All primary antibodies used in this study and their relevant dilutions are listed in Table 3. Secondary antibodies for IFM were Alexa-Fluor-488-conjugated donkey anti-mouse IgG, Alexa-Fluor-568-conjugated donkey anti-mouse IgG, Alexa-Fluor-488-conjugated donkey anti-rabbit IgG, Alexa-Fluor-568-conjugated goat anti-rabbit IgG, Alexa-Fluor-488-conjugated goat anti-rat IgG and Alexa-Fluor-568-conjugated goat anti-rat IgG, all diluted 1:600 and from Molecular Probes. Secondary antibodies for western blotting were alkaline-phosphatase-conjugated goat anti-mouse, goat anti-rabbit and goat anti-rat IgG all diluted 1:5000 (Sigma).

Immunofluorescence microscopy and live cell imaging

For immunofluorescence microscopy (IFM) of hFF, RPE, and NIH3T3 cells grown in six-well plates on glass cover slips, cells were fixed with methanol and formaldehyde and analyzed by IFM (Schneider et al., 2005; Schrøder et al., 2007). HBEC cells were fixed with cold methanol followed by 4% formaldehyde in PBS. For all IFM analyses, except those shown in Fig. 4 and Fig. 7G,H, cells were visualized on an Eclipse E600 microscope (Nikon) with EPI-FL3 filters and MagnaFire cooled CCD camera (Optronics, Goleta, CA, USA). Images shown in Fig. 4 were obtained using Zeiss LSM510 Meta laser scanning confocal microscope equipped with a 405 nm diode laser, a 488 nm argon laser and a 561 nm diode laser, and a 63× oil Plan-Apochromat n.a. 1.4 objective. *Z*-projections were generated using LSM software. For Fig. 7G,H, images were a taken on an Olympus BX63 upright, epi-fluorescence microscope. All images of RPE cells that express EB1-C, EB3-C and GFP were taken at an exposure time of 900 mseconds whereas images of siRNA-transfected hFF cells were taken at an exposure time of 430 mseconds. For quantification, fluorescent images of rootletin staining were processed using Olympus CellSens software by reducing background noise and increasing the signal of rootletin stained areas to fixed values for all images. This process assured that erroneous values due to out of focus centrosomes were not counted. The total area of rootletin staining for each cell was then measured using a built-in function of the CellSens software, whereby a threshold of detection was defined and applied to all images. Quantification of cilia was performed on formaldehyde-fixed IFM samples by randomly identifying cells through DAPI-staining and subsequently determining whether cilia were absent or present, as visualized with antibodies against Glu-tub or Arl13B. Adobe Photoshop CS4 version 11.0 (Adobe Systems Incorporated, San Jose, CA) was used for subsequent processing of all digital IFM images. Cilia length and inter-centriolar distances were measured on IFM images of fixed cells by using Image J software (http://rsb.info.nih.gov/ij/). Live cell imaging in CHO-K1 cells was done as described (Komarova et al., 2009).

Statistical analysis

Summary data are shown as the mean ± standard deviation (±s.d.) of at least three independent experiments. Unless otherwise mentioned, statistical analysis was carried out using the ANOVA test followed by the Tukey–Kramer method. *P*-values <0.05 indicate statistically significant differences.

Transmission electron microscopy

For transmission electron microscopy (TEM) analysis hFFs were cultured and transfected as for IFM, except that cells were grown in six-well plates on 22×22 mm

Aclar film pieces (Electron Microscopy Sciences, Hatfield, PA, USA). Cells were prefixed in culture medium with 2.5% glutaraldehyde, pH adjusted to 7.2, for 20 minutes at 37°C. Cells were then fixed in 0.1 M Hepes (pH 7.2), 4 mM $CaCl_2$, 2.5% glutaraldehyde (Serva Electrophoresis, Heidelberg, Germany) for 1 hour at room temperature plus 3 hours at 4°C. Fixative was replaced twice. Cells were postfixed with 1% OsO_4 for 45–60 minutes at 4°C and then incubated in 1% uranyl acetate for 60 minutes at 4°C. Between each step the samples were washed 3–4 times for 5 minutes each in 0.1 M HEPES (pH 7.2) containing 4 mM $CaCl_2$. Dehydration of the samples in ethanol, infiltration with Epon (Serva Electrophoresis) and flat embedding was performed by standard procedures (Geimer, 2009). Ultrathin serial sections (~60–70 nm) were cut with a diamond knife (type ultra 35°; Diatome, Biel, Switzerland) on a EM UC6 ultramicrotome (Leica, Wetzlar, Germany) and mounted on single-slot Pioloform-coated copper grids (Plano, Wetzlar, Germany). Sections were stained with uranyl acetate and lead citrate (Reynolds, 1963) and viewed with a JEM-2100 transmission electron microscope (JEOL, Tokyo, Japan) operated at 80 kV. Micrographs were taken using a 4000×4000 charge-coupled device camera (UltraScan 4000; Gatan, Pleasanton, CA) and Gatan Digital Micrograph software (version 1.70.16.). Image brightness and contrast were adjusted and figures assembled using Adobe Photoshop 8.0.1.

Purification of GST fusion proteins and protein interaction assays

Purification of GST fusion proteins, GST pull-down assays and mass spectrometry were done as described previously (Grigoriev et al., 2008), except that serum-starved RPE cells were used. For immunoprecipitation, serum-starved RPE cells were lysed in buffer containing 50 mM Tris pH 7.5, 150 mM NaCl, 0.5% NP-40, 1 mM $MgCl_2$, 0.1% sodium deoxycholate and a complete protease inhibitor cocktail, and the debris was pelleted by centrifugation. The lysate was incubated with protein G beads (Pierce) for 30 minutes at 4°C and the beads removed by centrifugation. The cleared lysate was incubated with antibodies against $p150^{Glued}$, EB1 or Nek2 (IgG control) for 1.5 hours at 4°C. Protein G beads were added and the mixture was incubated for another hour at 4°C. Beads were collected by centrifugation, washed three times for 10 minutes in buffer containing 20 mM Tris pH 7.4, 150 mM NaCl, and 0.5% Triton X-100, and proteins analysed by SDS-PAGE and immunoblotting.

SDS-PAGE and immunoblotting

Preparation of cell lysates for SDS-PAGE, measurement of protein concentrations, SDS-PAGE, electrophoretic transfer of proteins to nitrocellulose and immunoblotting were performed as described (Schrøder et al., 2007). Immunoblots were scanned and processed for publication in Adobe Photoshop CS4 version 11.0. Band intensities were analysed by densitometric scanning using UN-SCAN-IT 6.1 software (Silk Scientific Corp., Orem, UT, USA). For quantitative western blotting, linear standard curves were prepared using purified GST-EB fusion proteins (supplementary material Fig. S4A) and intensities of bands corresponding to native or GFP-tagged EB proteins were used to calculate the molar amounts of EB species in the lysates.

We thank Ewan E. Morrison, Erich A. Nigg, Kathryn Anderson, Klaus Yding Andersen and P. Hiemstra for reagents, J. Aarbiou and B. J. Scholte for performing ALI culture, Søren L. Johansen, Linda Schneider, Øjvind Moestrup, Michael Kosian, R. van der Linden and E. Dzierzak for technical assistance, and George B. Witman for helpful discussions. Supported by grants from the Danish Natural Science Research Council (272-05-0411 and 09-070398), the Novo Nordisk Foundation, the Danish Cancer Society, and the Lundbeck Foundation (L.B.P., S.T.C., S.F.P.) as well as the National Institutes of Health (RO1 HL103922) to Y.K. The PhD fellowship for J.M.S. was from the Faculty of Science, University of Copenhagen, J.L. and R.I.T. were suppoted by Novo Nordisk scholarships, and R.M. by a Fulbright scholarship. Deposited in PMC for release after 12 months.

Supplementary material available online at
http://jcs.biologists.org/cgi/content/full/124/15/2539/DC1

References

Akhmanova, A. and Steinmetz, M. O. (2008). Tracking the ends: a dynamic protein network controls the fate of microtubule tips. *Nat. Rev. Mol. Cell Biol.* **9**, 309-322.

Albrecht-Buehler, G. and Bushnell, A. (1980). The ultrastructure of primary cilia in quiescent 3T3 cells. *Exp. Cell Res.* **126**, 427-437.

Askham, J. M., Vaughan, K. T., Goodson, H. V. and Morrison, E. E. (2002). Evidence that an interaction between EB1 and $p150^{Glued}$ is required for the formation and maintenance of a radial microtubule array anchored at the centrosome. *Mol. Biol. Cell* **13**, 3627-3645.

Bahe, S., Stierhof, Y. D., Wilkinson, C. J., Leiss, F. and Nigg, E. A. (2005). Rootletin forms centriole-associated filaments and functions in centrosome cohesion. *J. Cell Biol.* **171**, 27-33.

Bahmanyar, S., Kaplan, D. D., Deluca, J. G., Giddings, T. H., Jr, O'Toole, E. T., Winey, M., Salmon, E. D., Casey, P. J., Nelson, W. J. and Barth, A. I. (2008). beta-Catenin is a Nek2 substrate involved in centrosome separation. *Genes Dev.* **22**, 91-105.

Ban, R., Matsuzaki, H., Akashi, T., Sakashita, G., Taniguchi, H., Park, S. Y., Tanaka, H., Furukawa, K. and Urano, T. (2009). Mitotic regulation of the stability of microtubule plus-end tracking protein EB3 by ubiquitin ligase SIAH-1 and Aurora mitotic kinases. *J. Biol. Chem.* **284**, 28367-28381.

Berbari, N. F., Lewis, J. S., Bishop, G. A., Askwith, C. C. and Mykytyn, K. (2008). Bardet-Biedl syndrome proteins are required for the localization of G protein-coupled receptors to primary cilia. *Proc. Natl. Acad. Sci. USA* **105**, 4242-4246.

Berbari, N. F., O'Connor, A. K., Haycraft, C. J. and Yoder, B. K. (2009). The primary cilium as a complex signaling center. *Curr. Biol.* **19**, R526-R535.

Blaineau, C., Tessier, M., Dubessay, P., Tasse, L., Crobu, L., Pagès, M. and Bastien, P. (2007). A novel microtubule-depolymerizing kinesin involved in length control of a eukaryotic flagellum. *Curr. Biol.* **17**, 778-782.

Bornens, M. (2002). Centrosome composition and microtubule anchoring mechanisms. *Curr. Opin. Cell Biol.* **14**, 25-34.

Busch, K. E. and Brunner, D. (2004). The microtubule plus end-tracking proteins mal3p and tip1p cooperate for cell-end targeting of interphase microtubules. *Curr. Biol.* **14**, 548-559.

Caspary, T., Larkins, C. E. and Anderson, K. V. (2007). The graded response to Sonic Hedgehog depends on cilia architecture. *Dev. Cell* **12**, 767-778.

Christensen, S. T., Pedersen, L. B., Schneider, L. and Satir, P. (2007). Sensory cilia and integration of signal transduction in human health and disease. *Traffic* **8**, 97-109.

Dammermann, A. and Merdes, A. (2002). Assembly of centrosomal proteins and microtubule organization depends on PCM-1. *J. Cell Biol.* **159**, 255-266.

Dawson, S. C., Sagolla, M. S., Mancuso, J. J., Woessner, D. J., House, S. A., Fritz-Laylin, L. and Cande, W. Z. (2007). Kinesin-13 regulates flagellar, interphase, and mitotic microtubule dynamics in Giardia intestinalis. *Eukaryot. Cell* **6**, 2354-2364.

De Groot, C. O., Jelesarov, I., Damberger, F. F., Bjelic, S., Scharer, M. A., Bhavesh, N. S., Grigoriev, I., Buey, R. M., Wuthrich, K., Capitani, G. et al. (2010). Molecular insights into mammalian end-binding protein heterodimerization. *J. Biol. Chem.* **285**, 5802-5814.

Etienne-Manneville, S., Manneville, J. B., Nicholls, S., Ferenczi, M. A. and Hall, A. (2005). Cdc42 and Par6-PKCzeta regulate the spatially localized association of Dlg1 and APC to control cell polarization. *J. Cell Biol.* **170**, 895-901.

Fliegauf, M., Benzing, T. and Omran, H. (2007). When cilia go bad: cilia defects and ciliopathies. *Nat. Rev. Mol. Cell Biol.* **8**, 880-893.

Follit, J. A., Tuft, R. A., Fogarty, K. E. and Pazour, G. J. (2006). The intraflagellar protein IFT20 is associated with the Golgi complex and is required for cilia assembly. *Mol. Biol. Cell* **17**, 3781-3792.

Fong, K. W., Hau, S. Y., Kho, Y. S., Jia, Y., He, L. and Qi, R. Z. (2009). Interaction of CDK5RAP2 with EB1 to track growing microtubule tips and to regulate microtubule dynamics. *Mol. Biol. Cell* **20**, 3660-3670.

Geimer, S. (2009). Immunogold labeling of flagellar components in situ. *Methods Cell Biol.* **91**, 63-80.

Geimer, S. and Melkonian, M. (2004). The ultrastructure of the *Chlamydomonas reinhardtii* basal apparatus: identification of an early marker of radial asymmetry inherent in the basal body. *J. Cell Sci.* **117**, 2663-2674.

Geraldo, S., Khanzada, U. K., Parsons, M., Chilton, J. K. and Gordon-Weeks, P. R. (2008). Targeting of the F-actin-binding protein drebrin by the microtubule plus-tip protein EB3 is required for neuritogenesis. *Nat. Cell Biol.* **10**, 1181-1189.

Gerdes, J., Lemke, H., Baisch, H., Wacker, H. H., Schwab, U. and Stein, H. (1984). Cell cycle analysis of a cell proliferation-associated human nuclear antigen defined by the monoclonal antibody Ki-67. *J. Immunol.* **133**, 1710-1715.

Graser, S., Stierhof, Y. D., Lavoie, S. B., Gassner, O. S., Lamla, S., Le Clech, M. and Nigg, E. A. (2007). Cep164, a novel centriole appendage protein required for primary cilium formation. *J. Cell Biol.* **179**, 321-330.

Grigoriev, I., Gouveia, S. M., van der Vaart, B., Demmers, J., Smyth, J. T., Honnappa, S., Splinter, D., Steinmetz, M. O., Putney, J. W., Jr, Hoogenraad, C. C. et al. (2008). STIM1 is a MT-plus-end-tracking protein involved in remodeling of the ER. *Curr. Biol.* **18**, 177-182.

Guarguaglini, G., Duncan, P. I., Stierhof, Y. D., Holmstrom, T., Duensing, S. and Nigg, E. A. (2005). The forkhead-associated domain protein Cep170 interacts with Polo-like kinase 1 and serves as a marker for mature centrioles. *Mol. Biol. Cell* **16**, 1095-1107.

Guirao, B., Meunier, A., Mortaud, S., Aguilar, A., Corsi, J. M., Strehl, L., Hirota, Y., Desoeuvre, A., Boutin, C., Han, Y. G. et al. (2010). Coupling between hydrodynamic forces and planar cell polarity orients mammalian motile cilia. *Nat. Cell Biol.* **12**, 341-350.

Hadjihannas, M. V., Bruckner, M. and Behrens, J. (2010). Conductin/axin2 and Wnt signalling regulates centrosome cohesion. *EMBO Rep.* **11**, 317-324.

Hashimoto, M., Shinohara, K., Wang, J., Ikeuchi, S., Yoshiba, S., Meno, C., Nonaka, S., Takada, S., Hatta, K., Wynshaw-Boris, A. et al. (2010). Planar polarization of node cells determines the rotational axis of node cilia. *Nat. Cell Biol.* **12**, 170-176.

Hayashi, I. and Ikura, M. (2003). Crystal structure of the amino-terminal microtubule-binding domain of end-binding protein 1 (EB1). *J. Biol. Chem.* **278**, 36430-36434.

Honnappa, S., John, C. M., Kostrewa, D., Winkler, F. K. and Steinmetz, M. O. (2005). Structural insights into the EB1-APC interaction. *EMBO J.* **24**, 261-269.

Ishikawa, H., Kubo, A. and Tsukita, S. (2005). Odf2-deficient mother centrioles lack distal/subdistal appendages and the ability to generate primary cilia. *Nat. Cell Biol.* **7**, 517-524.

Juwana, J. P., Henderikx, P., Mischo, A., Wadle, A., Fadle, N., Gerlach, K., Arends, J. W., Hoogenboom, H., Pfreundschuh, M. and Renner, C. (1999). EB/RP gene family encodes tubulin binding proteins. *Int. J. Cancer* **81**, 275-284.

Kim, J., Krishnaswami, S. R. and Gleeson, J. G. (2008). CEP290 interacts with the centriolar satellite component PCM-1 and is required for Rab8 localization to the primary cilium. *Hum. Mol. Genet.* **17**, 3796-3805.
Kim, J. C., Badano, J. L., Sibold, S., Esmail, M. A., Hill, J., Hoskins, B. E., Leitch, C. C., Venner, K., Ansley, S. J., Ross, A. J. et al. (2004). The Bardet-Biedl protein BBS4 targets cargo to the pericentriolar region and is required for microtubule anchoring and cell cycle progression. *Nat. Genet.* **36**, 462-470.
Knödler, A., Feng, S., Zhang, J., Zhang, X., Das, A., Peränen, J. and Guo, W. (2010). Coordination of Rab8 and Rab11 in primary cilia biogenesis. *Proc. Natl. Acad. Sci. USA* **107**, 6346-6351.
Knudsen, E. S. and Wang, J. Y. (1997). Dual mechanisms for the inhibition of E2F binding to RB by cyclin-dependent kinase-mediated RB phosphorylation. *Mol. Cell. Biol.* **17**, 5771-5783.
Komarova, Y., Vorobjev, I. A. and Borisy, G. G. (2002). Life cycle of MTs: persistent growth in the cell interior, asymmetric transition frequencies and effects of the cell boundary. *J. Cell Sci.* **115**, 3527-3539.
Komarova, Y., Lansbergen, G., Galjart, N., Grosveld, F., Borisy, G. G. and Akhmanova, A. (2005). EB1 and EB3 control CLIP dissociation from the ends of growing microtubules. *Mol. Biol. Cell* **16**, 5334-5345.
Komarova, Y., De Groot, C. O., Grigoriev, I., Gouveia, S. M., Munteanu, E. L., Schober, J. M., Honnappa, S., Buey, R. M., Hoogenraad, C. C., Dogterom, M. et al. (2009). Mammalian end binding proteins control persistent microtubule growth. *J. Cell Biol.* **184**, 691-706.
Kubo, A., Sasaki, H., Yuba-Kubo, A., Tsukita, S. and Shiina, N. (1999). Centriolar satellites: molecular characterization, ATP-dependent movement toward centrioles and possible involvement in ciliogenesis. *J. Cell Biol.* **147**, 969-980.
Lee, T., Langford, K. J., Askham, J. M., Bruning-Richardson, A. and Morrison, E. E. (2008). MCAK associates with EB1. *Oncogene* **27**, 2494-2500.
Liu, Q., Tan, G., Levenkova, N., Li, T., Pugh, E. N., Jr, Rux, J., Speicher, D. W. and Pierce, E. A. (2007). The proteome of the mouse photoreceptor sensory cilium complex. *Mol. Cell. Proteomics* **6**, 1299-1317.
Louie, R. K., Bahmanyar, S., Siemers, K. A., Votin, V., Chang, P., Stearns, T., Nelson, W. J. and Barth, A. I. (2004). Adenomatous polyposis coli and EB1 localize in close proximity of the mother centriole and EB1 is a functional component of centrosomes. *J. Cell Sci.* **117**, 1117-1128.
Marshall, W. F. and Rosenbaum, J. L. (2001). Intraflagellar transport balances continuous turnover of outer double microtubules: implications for flagellar length control. *J. Cell Biol.* **155**, 405-414.
Mirzadeh, Z., Han, Y. G., Soriano-Navarro, M., Garcia-Verdugo, J. M. and Alvarez-Buylla, A. (2010). Cilia organize ependymal planar polarity. *J. Neurosci.* **30**, 2600-2610.
Mogensen, M. M., Malik, A., Piel, M., Bouckson-Castaing, V. and Bornens, M. (2000). Microtubule minus-end anchorage at centrosomal and non-centrosomal sites: the role of ninein. *J. Cell Sci.* **113**, 3013-3023.
Molla-Herman, A., Ghossoub, R., Blisnick, T., Meunier, A., Serres, C., Silbermann, F., Emmerson, C., Romeo, K., Bourdoncle, P., Schmitt, A. et al. (2010). The ciliary pocket: an endocytic membrane domain at the base of primary and motile cilia. *J. Cell Sci.* **123**, 1785-1795.
Nachury, M. V., Loktev, A. V., Zhang, Q., Westlake, C. J., Peranen, J., Merdes, A., Slusarski, D. C., Scheller, R. H., Bazan, J. F., Sheffield, V. C. et al. (2007). A core complex of BBS proteins cooperates with the GTPase Rab8 to promote ciliary membrane biogenesis. *Cell* **129**, 1201-1213.
Nachury, M. V., Seeley, E. S. and Jin, H. (2010). Trafficking to the ciliary membrane: how to get across the periciliary diffusion barrier? *Annu. Rev. Cell Dev. Biol.* **26**, 59-87.
Paintrand, M., Moudjou, M., Delacroix, H. and Bornens, M. (1992). Centrosome organization and centriole architecture: their sensitivity to divalent cations. *J. Struct. Biol.* **108**, 107-128.
Pazour, G. J. and Bloodgood, R. A. (2008). Targeting proteins to the ciliary membrane. *Curr. Top. Dev. Biol.* **85**, 115-149.
Pedersen, L. B. and Rosenbaum, J. L. (2008). Intraflagellar transport (IFT): role in ciliary assembly, resorption and signalling. *Curr. Top. Dev. Biol.* **85**, 23-61.
Pedersen, L. B., Geimer, S., Sloboda, R. D. and Rosenbaum, J. L. (2003). The microtubule plus end-tracking protein EB1 is localized to the flagellar tip and basal bodies in *Chlamydomonas reinhardtii*. *Curr. Biol.* **13**, 1969-1974.
Pedersen, L. B., Veland, I. R., Schrøder, J. M. and Christensen, S. T. (2008). Assembly of primary cilia. *Dev. Dyn.* **237**, 1993-2006.
Piao, T., Luo, M., Wang, L., Guo, Y., Li, D., Li, P., Snell, W. J. and Pan, J. (2009). A microtubule depolymerizing kinesin functions during both flagellar disassembly and flagellar assembly in Chlamydomonas. *Proc. Natl. Acad. Sci. USA* **106**, 4713-4718.
Piel, M., Meyer, P., Khodjakov, A., Rieder, C. L. and Bornens, M. (2000). The respective contributions of the mother and daughter centrioles to centrosome activity and behavior in vertebrate cells. *J. Cell Biol.* **149**, 317-330.
Reynolds, E. S. (1963). The use of lead citrate at high pH as an electron-opaque stain in electron microscopy. *J. Cell Biol.* **17**, 208-212.
Sandblad, L., Busch, K. E., Tittmann, P., Gross, H., Brunner, D. and Hoenger, A. (2006). The Schizosaccharomyces pombe EB1 homolog Mal3p binds and stabilizes the microtubule lattice seam. *Cell* **127**, 1415-1424.
Schneider, L., Clement, C. A., Teilmann, S. C., Pazour, G. P., Hoffmann, E. K., Satir, P. and Christensen, S. T. (2005). PDGFRαα signaling is regulated through the primary cilium in fibroblasts. *Curr. Biol.* **15**, 1861-1866.
Schrøder, J. M., Schneider, L., Christensen, S. T. and Pedersen, L. B. (2007). EB1 is required for primary cilia assembly in fibroblasts. *Curr. Biol.* **17**, 1134-1139.
Schuyler, S. C. and Pellman, D. (2001). Microtubule "plus-end-tracking-proteins": the end is just the beginning. *Cell* **105**, 421-424.
Skube, S. B., Chaverri, J. M. and Goodson, H. V. (2010). Effect of GFP tags on the localization of EB1 and EB1 fragments in vivo. *Cytoskeleton* **67**, 1-12.
Slep, K. C., Rogers, S. L., Elliott, S. L., Ohkura, H., Kolodziej, P. A. and Vale, R. D. (2005). Structural determinants for EB1-mediated recruitment of APC and spectraplakins to the microtubule plus end. *J. Cell Biol.* **168**, 587-598.
Sorokin, S. (1962). Centrioles and the formation of rudimentary cilia by fibroblasts and smooth muscle cells. *J. Cell Biol.* **15**, 363-377.
Stepanova, T., Slemmer, J., Hoogenraad, C. C., Lansbergen, G., Dortland, B., De Zeeuw, C. I., Grosveld, F., van Cappellen, G., Akhmanova, A. and Galjart, N. (2003). Visualization of microtubule growth in cultured neurons via the use of EB3-GFP (end-binding protein 3-green fluorescent protein). *J. Neurosci.* **23**, 2655-2664.
Su, L. K. and Qi, Y. (2001). Characterization of human MAPRE genes and their proteins. *Genomics* **71**, 142-149.
Tirnauer, J. S., Grego, S., Salmon, E. D. and Mitchison, T. J. (2002). EB1-microtubule interactions in *Xenopus* egg extracts: role of EB1 in microtubule stabilization and mechanisms of targeting to microtubules. *Mol. Biol. Cell* **13**, 3614-3626.
van Wetering, S., Zuyderduyn, S., Ninaber, D. K., van Sterkenburg, M. A., Rabe, K. F. and Hiemstra, P. S. (2007). Epithelial differentiation is a determinant in the production of eotaxin-2 and -3 by bronchial epithelial cells in response to IL-4 and IL-13. *Mol. Immunol.* **44**, 803-811.
Vitre, B., Coquelle, F. M., Heichette, C., Garnier, C., Chretien, D. and Arnal, I. (2008). EB1 regulates microtubule dynamics and tubulin sheet closure in vitro. *Nat. Cell Biol.* **10**, 415-421.
Vorobjev, I. A., Rodionov, V. I., Maly, I. V. and Borisy, G. G. (1999). Contribution of plus and minus end pathways to microtubule turnover. *J. Cell Sci.* **112**, 2277-2289.
Watson, P. and Stephens, D. J. (2006). Microtubule plus-end loading of p150(Glued) is mediated by EB1 and CLIP-170 but is not required for intracellular membrane traffic in mammalian cells. *J. Cell Sci.* **119**, 2758-2767.
Wen, Y., Eng, C. H., Schmoranzer, J., Cabrera-Poch, N., Morris, E. J., Chen, M., Wallar, B. J., Alberts, A. S. and Gundersen, G. G. (2004). EB1 and APC bind to mDia to stabilize microtubules downstream of Rho and promote cell migration. *Nat. Cell Biol.* **6**, 820-830.
Westlake, C. J., Baye, L. M., Nachury, M. V., Wright, K. J., Ervin, K. E., Phu, L., Chalouni, C., Beck, J. S., Kirkpatrick, D. S., Slusarski, D. C. et al. (2011). Primary cilia membrane assembly is initiated by Rab11 and transport particle II (TRAPPII) complex-dependent trafficking of Rabin8 to the centrosome. *Proc. Natl. Acad. Sci. USA* **108**, 2759-2764.
Yan, X., Habedanck, R. and Nigg, E. A. (2006). A complex of two centrosomal proteins, CAP350 and FOP, cooperates with EB1 in microtubule anchoring. *Mol. Biol. Cell* **17**, 634-644.
Yang, J., Gao, J., Adamian, M., Wen, X. H., Pawlyk, B., Zhang, L., Sanderson, M. J., Zuo, J., Makino, C. L. and Li, T. (2005). The ciliary rootlet maintains long-term stability of sensory cilia. *Mol. Cell. Biol.* **25**, 4129-4137.
Zhou, F. Q., Zhou, J., Dedhar, S., Wu, Y. H. and Snider, W. D. (2004). NGF-induced axon growth is mediated by localized inactivation of GSK-3beta and functions of the microtubule plus end binding protein APC. *Neuron* **42**, 897-912.

Journal of Cell Science